Tailoring piezoresistive response of carbon nanotubes sensors by hybridization of cellulose nanocrystals for composite structures

Adel Alrai[a,b], Ersin Beyhan[a,b], Amir Asadi[c], Elif Özden-Yenigün[d], Hülya Cebeci[a,b,*]

[a] Department of Aeronautics and Astronautics, Istanbul Technical University, 34469, Turkey

[b] Aerospace Research Center, Istanbul Technical University, 34467, Turkey

[c] Department of Engineering Technology & Industrial Distribution, Texas A&M University, College Station, TX 77843-3367, USA

[d] School of Design, Textiles, Royal College of Art, SW7 2EU, UK

* Corresponding author. Faculty of Aeronautics and Astronautics, Istanbul Technical University, 34467, Turkey.

E-mail address: hulya.cebeci@itu.edu.tr

Abstract

Here, the piezoresistive behavior and the underlying sensing mechanism of carbon nanotubes (CNTs) and cellulose nanocrystals (CNCs) composite strain sensors were studied. Aqueous CNT/CNC inks were developed, characterized, and applied on the surface of glass fiber reinforced polymer (GFRP) composites to function as strain sensors. The sensor's behavior and sensitivities at small and large strains depended on the initial composition of CNCs. The sensor with a CNT/CNC composite with composition of 0.8:0.4 (wt.%:wt.%) had gauge factors of 0.9 and 6.4 at 0.60 and 1.35 % strains, respectively. At higher composition of 0.8:4.0 (wt.%:wt.%), gauge factors of 0.5 and 22.2 were calculated for the same strain regions. Through analytical model and morphology analyses, we discussed the influence of CNCs on CNT contact types and on the average tunneling distance between CNTs and the their piezoresistive performance. It was also discussed that CNC particles control the types of contacts between adjacent CNTs. As a result, tailoring piezoresistive behavior was demonstrated. In conclusion, applying a binder-free and environmentally friendly sustainable aqueous ink on a surface of a composite was revealed to be an effective and practical approach for tailored strain sensing.

Keywords: Hybridization, Carbon nanotube, Cellulose nanocrystals, Composites, Piezoresistive.

1. Introduction

Monitoring strain sensors currently in use for composites face obstacles that require the need for a better alternative. Optical fiber sensors, *e.g.,* fiber Bragg grating (FBG), one of the widely used technology [1], incorporated with composites, are only sensitive to localized damages and require noise-canceling analysis to enhance their performance [2]. The presence of the fiber in the matrix composite facilitates the rise of stress raisers that lead to complications [3–5]. Advanced sensors polymeric sensors have also been proposed for various application [6]. In the last decade, piezoresistive carbon-based nanomaterial strain sensors emerged as a potential alternative [7].

Two approaches are adopted to utilize conductive nanomaterials for piezoresistive strain sensor applications for composites. The first one is to integrate electrically conductive nanofillers into the matrix of composites in which the sensing mechanism and sensitivity rely on the nanofillers' dispersion quality, dimensions, and geometries. To demonstrate the effect of filler geometry, Paleari et al. studied glass fiber reinforced polymers (GFRPs) reinforced with carbon black (CBs) and carbon nanotubes (CNTs) [8]. CBs reinforced GFRP resulted in a gauge factor of 6 at 6.0 wt.% of CBs, whereas 1.0 wt.% CNTs reinforced GFRP resulted in a gauge factor of 1. Spherical fillers like CBs have higher sensitivity than 1D fillers and CNTs; however, they have a higher percolation threshold. Yazdani et al. demonstrated that the difference in the sensor sensitivity was attributed to the faster deconstruction of the conductive network in CB compared with CNTs which require higher strain for separation [9]. Other works focused on coating glass fibers with 2D nanomaterials such graphene and compared their piezoresistive response with that of CNT-coated fiber composite [5,10]. Due to fabrication complication and dispersion issues, the previous attempts, however, could jeopardize mechanical property [5].

To avoid the challenge arising from dispersing particulates into polymer matric, several studies have embedded carbon nanotube films, referred to as CNT buckypapers (CNT BPs), into composites. Different types of CNTs, such as single-walled nanotubes (SWCNTs) and multi-walled nanotubes (MWCNTs), have been used to investigate their performance [11,12]. It was concluded that sensing performance relied upon strain levels in CNT BPs sensors [2]. Initially, at low strains in the elastic region, the deconstruction and reconstruction of the conductive paths and electron tunneling are the dominant changes in the CNT BP. At high strains, however, deconstruction is the dominant intrinsic change. Under a three-point bending test and at a small strain, sensitivity as high as 46 was calculated [2]. CNT BPs as interlayers in composites have also been used to quantify damages and improve fatigue resistance in GFRP laminates [11].

The Piezoresistivity of strain sensors incorporated in composites depends not only on the fillers' properties but also on the composite matrix properties and processing conditions [13]. De Vivo et al. showed that tunneling conductivity decreased as the barrier height of the polymer matrix increased [14]. Hu et al. demonstrated that regardless of the CNT ratio, the sensitivity of CNT nanocomposite sensors was inversely proportional to curing temperature and directly proportional to mixing rate [15,16]. That was attributed to the complex relation between effective network formulation among nanofillers and processing conditions.

In the past few years, the emerging hybrid composite of cellulose nanocrystals (CNC) with CNTs has gained the attention of some researchers due to its great potential in various applications, such as flexible sensors, patch antennas, and structural applications [17–21]. CNT/CNC dispersion is highly stable in water for over six months [19] because of high charges on the surface of the CNCs [22,23] and covalent bond formation between CNTs and CNCs [24]. Wang et al. demonstrated that CNT/CNC hybrid reinforcement nanocomposites decreased the electrical percolation

threshold by four folds compared to pristine CNT polymer nanocomposites [17]. The strain sensitivity of the CNT/CNC nanocomposite sensor was 43.5 at a strain of 100%. These results were attributed to CNCs' ability to homogenously disperse CNTs in the matrix and prevent CNTs from excessive slippage. To our knowledge, detailed studies on the strain sensing mechanism and performance of CNT/CNC composite prepared from inks are still lacking.

In this study, the piezoresistive behavior and the underlying sensing mechanism of highly sensitive CNT/CNC composite strain sensors were studied. First, aqueous CNT/CNC inks were developed, characterized, and applied onto composites to function as strain sensors. The rheological behavior of the developed ink was investigated. Next, the piezoresistive behaviors of different CNT/CNC composites were investigated in tensile and cyclic tensile modes. A modification of an analytical model was also provided to correlate the theory with the experimental findings. The sensor's behavior at small and large strains and sensitivities depended on the initial composition of CNCs. Gauge factor as high as 1.0 was calculated for the elastic region for CNT/CNC composition of 0.5:0.5 (wt.%:wt.%), and a gauge factor of 22.2 was calculated for the plastic region for CNT/CNC composition of 0.8:4.0 (wt.%:wt.%). It was demonstrated that CNC particles could control the type of contacts between CNTs and their average tunneling distance. The reliable performance of CNT/CNC strain sensors of different compositions was tested under cyclic test mode, which showed a negative piezoresistive behavior and was stable after a few cycles. It is concluded that the piezoresistive behavior of the CNT/CNC composite sensor and average tunneling distance is controllable by manipulating the initial composition of the CNT/CNC inks, and a proposed mechanism was provided. Also, applying a binder-free and environmentally friendly sustainable aqueous ink on a surface of a composite was demonstrated to be an effective and practical approach to be functionalized as a strain sensor. The process eliminates the need for processing conditions,

e.g. mixing rate, curing temperature, and matrix properties, which render the method to be, perhaps, more favorable than already studied piezoresistive sensors.

2. Experimental

2.1.Materials

Distilled water was generated through NUVE model NS 103. CNTs with a diameter of 6-9 nm, a length of 5 μm, and a purity of 95% were purchased from Sigma-Aldrich (USA). Cellulose nanocrystals, NCV-100, were purchased from CelluForce (Canada). Epoxy resin LR160 and hardener LH160 (weight ratio of resin/hardener is 100:25) were purchased from Dost Kimya, Hexion (Turkey). Plane woven E-Glass fabric (GF) with a density of 200 g/m^2 was purchased from Hexcel (USA). The silver paste was purchased from Nanografi (Turkey). All materials were used without further purification.

2.2.Preparation of CNT/CNC inks and Fabrication of CNT/CNC sensors

The prepared inks were made of CNTs, CNCs, and distilled water. First, based on the final desired concentration, the required weight of CNCs was added to a predetermined amount of water and then ultrasonicated for at least 15 minutes using microtip sonication (Sonics VCX750). Next, the corresponding weight of CNTs was added to the mixture and ultrasonicated for at least 60 minutes, depending on the ink concentration. Details on sample coding and the concentration of tested inks can be found in Table 1.

The as-prepared inks were applied on the rough surface of the composite using a coating roller. The ink was applied in the center of the coupons with a total area of 25×40 mm^2 and was dried at 40°C for 2 hours. Electrodes, copper foils with a thickness of 0.1 mm, with a total area of 5×25 mm^2 were attached to the far edges of the dried surface of the ink using electrically conductive silver paste. The prepared system was placed in a furnace at 40°C for 10 hours to ensure maximum

performance of the silver paste. Depending on the CNT/CNC composition, the developed sensors were designated with the following abbreviations. For example, the strain sensor that was prepared from 0.5 wt.% CNT and 0.5 wt.% is referred to as CNT/CNC@0.5:0.5 sensors.

Table 1: Sample identification for developed CNT/CNC inks and abbreviations.

Total weight percentage (wt.%) of CNT and CNC	CNT/CNC weight ratio (wt.%:wt.%)	Applicability of the ink	Abbreviated strain sensor
4.0	0.0:4.0	N/A*	-
0.2	0.1:0.1	N/A*	-
1.0	0.5:0.5	Applicable**	CNT/CNC@0.5:0.5
1.2	0.8:0.4	Applicable**	CNT/CNC@0.8:0.4
1.6	0.8:0.8	Applicable**	CNT/CNC@0.8:0.8
4.8	0.8:4.0	Applicable**	CNT/CNC@0.8:4.0

* N/A: not applicable, ** Applicable: The ink's concentration was suitable for coating on the surface of the composite

2.3.Preparation of GFRP composite

A total of five bidirectional GF plies were used to fabricate all the composites in this study. The GF-reinforced polymer (GFRP) laminates were prepared using vacuum infusion. 4:1 weight ratio of resin to hardener was thoroughly mixed and degassed for ten minutes before infusing into the vacuum bag. All the GFRP composites were cured at room temperature for 24 hours. Before subsequent use, the as-prepared GFRP composites were cut into 25×250 mm^2 as coupons.

2.4.Characterization methods

2.4.1. Rheology behavior

The rheology behavior of the developed inks was studied using a parallel plate rheometer instrument (Discovery Hybrid Rheometer 2, TA Instruments). 0.5 mL of the freshly prepared ink

was placed on the stationary plate, and a gap of 1 mm between the fixed and rotary plates was set. First, a strain sweep test was conducted, from which the linear viscoelastic region was determined. Next, a frequency sweep test in the range of 0.1 to 628 rad/sec was performed to measure the complex viscosity. All tests were carried out at room temperature.

2.4.2. Morphology

The surface morphology of the developed CNT/CNC strain sensors was investigated using Scanning Electron Microscopy (SEM) (FEI, model Quanta FEG 450, Austria), operating at 10 kV. To avoid charging effects, the specimens were sputtered with a thin layer of Au.

2.4.3. Tensile test of GFRP composite

A tensile test was conducted on neat GFRPs using a Universal Testing Machine (UTM) (AGS-X, Shimadzu) equipped with a 50 kN load cell. The test was performed following the ASTM D3039 standard. Briefly, a fabricated coupon (25×250 mm^2) was mounted between the grips at a distance of 150 mm, and crosshead speed was set at 2 mm/min. During testing, first, using a contact extensometer (Epsilon, Model 3542, USA), the tensile test was carried out up to 0.7 mm. Next, the extensometer was removed to prevent potential damage to the contact extensometer, and tensile tests continued until failure.

2.4.4. Electromechanical testing

Electromechanical testing is demonstrated in Schematic 1. The setup consisted of a UTM and a source meter unit (200V, 1A, 20W, Keithley 2400). After the CNT/CNC-coated composite was mounted in the UTM, a constant voltage of 2.1 V was applied, and a two-wire configuration was adopted. The data of resistance were collected by LabTracer software. The maximum allowed extension measured by the contact extensometer was 0.7 mm. In tensile testing, the crosshead speed was 2 mm/min; in cyclic tensile testing, the crosshead speed was 6 mm/min.

It is worth reporting that some of the developed strain sensors required a stabilization period (See Electromechanical analysis section) while under a voltage difference. Therefore, for the sake of consistency, after the voltage difference was applied and before mechanical testing, all strain sensors were allowed to be under constant voltage for a brief time (five minutes) to reach stabilization. The electrical resistance sampling frequency was 1 Hz.

It is worth reporting that a preliminary study was carried out to determine whether or not an electrical resistance sampling frequency of 1 Hz was enough to capture the intrinsic changes occurring on the strain during mechanical testing. Using CNT/CNC@0.5:0.5 sensors as a reference, cyclic tests were performed by varying electrical resistance sampling frequencies at 1 and 20 Hz. Figure S1 shows that by increasing the sampling frequency from 1 to 20 Hz for cyclic tests, the accuracy of the test did not change, emphasizing that 1 Hz was enough to capture the intrinsic changes occurring on the strain during mechanical tests.

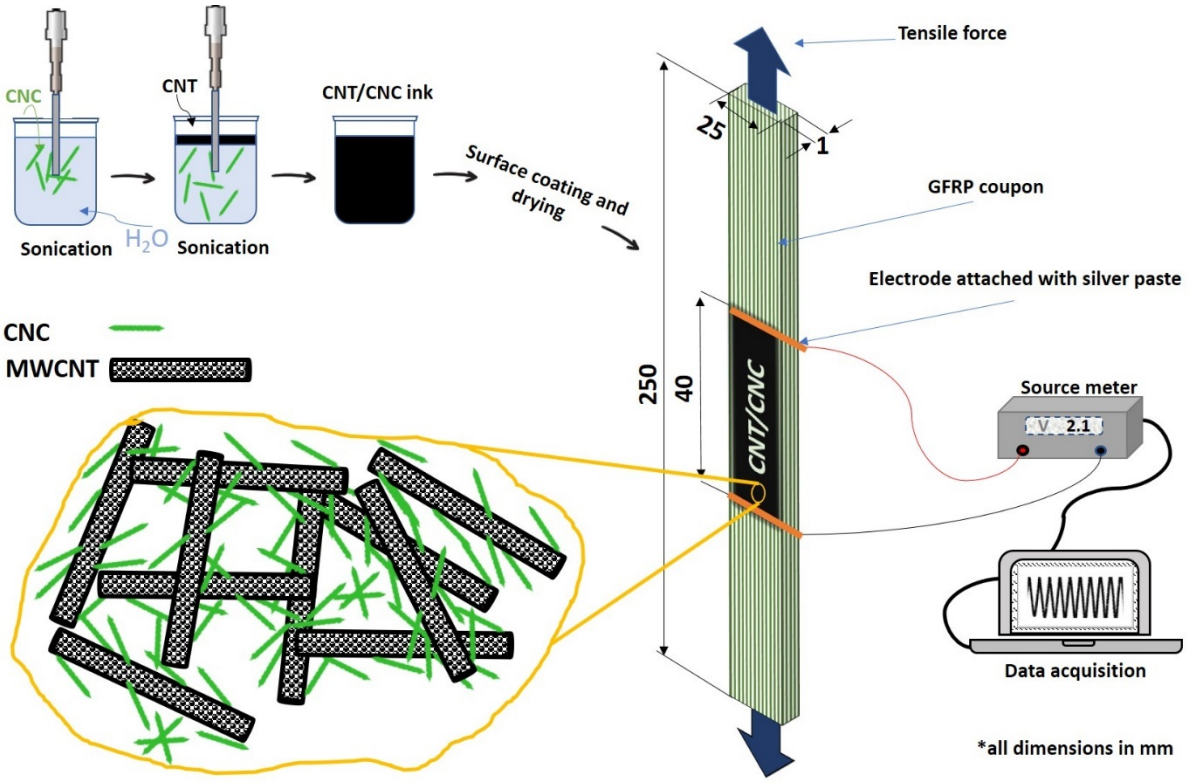

Schematic 1: Preparation of CNT/CNC applied onto GFRP as paint and schematics of the testing setup.

2.5. Analytical modeling

The contact resistance between CNTs is usually much higher than the intrinsic resistance of a CNT [25], thus, the resistance of CNT composites can be approximated by the following equation [25]

$$R = \frac{M}{N}\frac{h^2 t}{d^2 e^2 \sqrt{2m\chi}} \exp\left[4\frac{\pi t}{h}\sqrt{2m\chi}\right] \qquad \text{Equation (1)}$$

where M, N, h, t, d, e, m, and χ denote number of CNTs in a conductive path, the number of conductive paths, Planck's constant, average tunneling distance, the diameter of CNT, electron charge, the mass of electron, and work function of a CNT, respectively. The attachment of CNCs to a CNT was shown not to increase the intrinsic resistance of a CNT (See section 3.3 Electromechanical analysis), which further justifies ignoring intrinsic resistance in Equation 1. However, Equation 1 does not consider the effect of hybridization on the available tunneling junctions. So, by considering the effective length of a CNC and a constant related to the initial content of CNC, the following modification was suggested

$$\frac{M}{N}\frac{d^2}{Z(d + 2l_{eff}^{CNC})^2}$$

where l_{eff}^{CNC} is the effective length of a CNC, and Z is a constant which depends on the number of CNCs, *i.e.,* concentration and/or agglomeration. l_{eff}^{CNC} is the projection of actual CNC length on the axis, perpendicular to MWCNT, best illustrated in Schematic 2. l_{eff}^{CNC} was calculated as $l_{eff}^{CNC} = l^{CNC}\sin$ (ß) where l^{CNC} is the average length of a CNC rod, and ß is the average angle between a CNC rod and a CNT, which depends on the surface charge of the CNC and defect sites on the CNT [23]. In this work, as was recently demonstrated that CNCs attach with their tips on MWCNT

rather than a perfect alignment [24], therefore, the average ß was accepted to be 45° without considering any other parametric studies.

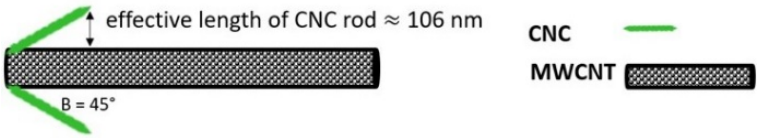

Schematic 2: Illustration of the effective length of a CNC rod.

Equation 1 can be rewritten as

$$R = \frac{M}{N}\frac{h^2 t}{Z(d + 2l^{CNC}\sin(ß))^2 e^2\sqrt{2m\chi}}\exp\left[4\frac{\pi t}{h}\sqrt{2m\chi}\right] \qquad \text{Equation (2)}$$

To emphasize the effect of CNC on initial tunneling distance, Equation 2 was arranged as the following

$$t_0 = \frac{h}{e^2\sqrt{2m\chi}}W\left(e^2\sqrt{2m\chi}\frac{N}{M}\frac{Z(d + 2l^{CNC}\sin(ß))^2}{h^2}\rho_0\right) \qquad \text{Equation (3)}$$

where $W(x)$ and ρ_0 are the Lambert function [25] and resistivity, respectively. Equation 3 shows that the initial tunneling resistance is proportional to the length of the CNC rod, the angle between a CNC and a CNT, and the content of the CNCs. These three parameters affect the tunneling junctions between CNTs.

In literature, change in average tunneling distance, t, has a linear relation with strain [26,27]. However, in the case of CNT/CNC, it was suggested that change in average tunneling distance has nonlinear relation with strain as the following

$$t = t_0(1 + E\varepsilon^B) \qquad \text{Equation (4)}$$

where ε is strain, and B is constant and is related to the initial CNC content. E is a constant and can be calculated as the following

$$E = cos^2 a - \nu\, sin^2 a \qquad \text{Equation (5)}$$

where ν is Poisson's ratio which was taken to be 0.31 [28,29] and a is the angle between the direction of strain and tunneling distance [30]. For random orientation of CNTs, the value of a is assumed to be constant during the tensile test and evaluated to be $a = sin^{-1}\frac{\pi}{4}$ [30,31]. The final value of E was calculated to be 0.345.

Change of resistance can be calculated as the following [14]

$$\frac{\Delta R}{R_0} = \frac{R_t}{R_0} - 1 = \left(\frac{\mathrm{t}}{t_0}\right)\exp\left[\frac{4\pi\sqrt{2m\chi}}{h}(t - t_0)\right] - 1 \qquad \text{Equation (6)}$$

It should be emphasized that the terms Z, l^{CNC}, and sin(ß) do not appear in Equation 6 because they are constants and do not depend on the change in strain. Rearranging Equation 4 and combining it with Equation 6, we have

$$\frac{\Delta R}{R_0} = (1 + E\varepsilon^B)\exp\left[\frac{4\pi\sqrt{2m\chi}}{h}t_0 E\varepsilon^B\right] - 1 \qquad \text{Equation (7)}$$

Plugging the value of the constants in Equation 7 (See Table 2), we have

$$\frac{\Delta R}{R_0} = (1 + 0.345\varepsilon^B)\exp[1.58t_0\varepsilon^B] - 1 \qquad \text{Equation (8)}$$

Table 2: Constants and parameters used in this study for modeling.

Constants	h	e	m	χ*	d	l^{CNT}	l^{CNC}
Value	6.62×10^{-34}	1.602×10^{-19}	9.109×10^{-31}	0.2	7.5	5000	150
Unit	Joule-second	Coulombs	Kg	eV	nm	nm	nm

*in absence of polymer matrix, the barrier height was assumed to be 0.2 eV [32–34] and to be constant with increase or decrease of CNC.

3. Results and Discussion

Depending on crystallinity degree of CNC and humidity level, CNC retains water in its crystalline structure, albeit at lower rate compared with amorphous cellulose [35]. In this study the water content in the prepared sensors was assumed to be between 0 – 5% [35,36], thus, since all test tests were done in the same environment under humidity of approximately 50% or less, hence, minor effect on the evaluation of the sensors was assumed. The effect of humidity on sensors' performance was not investigated in this work, but it is the subject of future research.

The surface chemistry of CNCs has two different chemical affinities; hydrophilic and hydrophobic, which result from a hydroxyl group, and C-H moieties, which can stabilize water-oil interfaces [37]. CNC is derived from naturally occurring substances such as wood and cotton, which renders it a sustainable substance [38,39]. Conversely, CNT has a high aspect ratio, is highly conductive, and is hydrophobic. In addition to Van der Waals strong interaction, the hydrophobicity of CNTs results in their agglomeration in a water-based solution. However, it has been demonstrated successfully that to disperse CNTs in an aqueous solution, CNCs are excellent nanoparticles to overcome the challenge because of their surface chemistry [40]. CNCs disperse MWCNT in water due to hydrophobic interactions and covalent bond formation among the two particles [22–24]. Because of the defects associated with the side walls of MWCNT, which may lead to hydrophilic sites [23], only the CNC tip interacts with the sp^2 carbon lattice as opposed to the nearly perfect alignment between CNC and SWCNT [19]. That was because the side walls of SWCNT are of higher hydrophobicity compared with MWCNT. Also, it was shown recently that the tips of CNCs are more likely to attach to the side walls of MWCNT compared with perfect alignment due to a covalent bond formed between the defects of MWCNT and the hydroxyl groups on the CNCs [24]. The effect of CNT and CNC interaction in an aqueous medium on rheological properties were investigated.

3.1.Rheology behavior of CNT/CNC inks

To understand the rheological relation between CNT and CNC in aqueous ink, it is essential to understand the rheological behavior of plain CNC aqueous solutions. Therefore, a CNC-based aqueous solution with 4.0 wt.% concertation was tested initially since it is the highest ratio of CNC used in the developing CNT/CNC inks. The result is summarized in Table 3. Three distinct regions were identified. First, at low shear rates (smaller than one 1/s), it was shown that as the shear rate increased noticeable decrease in viscosity was noted, indicating shear thinning behavior as shown in Figure 1a. At a slightly higher shear rate, a plateau was observed. At a higher shear rate decrease in viscosity was observed again. This behavior is typical for liquid crystal solutions [41], and, more importantly, similar behavior of CNC aqueous solution was reported [39–42].

Table 3: Rheological properties of CNT/CNC inks at varying weight ratios.

CNT/CNC weight ratio (wt.%:wt.%)	Shear viscosity* (Pa.s)
0.0:4.0	0.35
0.1:0.1	2.29
0.5:0.5	8.83
0.8:0.4	86.54
0.8:0.8	110.33
0.8:4.0	222.06

* shear viscosity at a constant shear rate of 0.1 rad/sec

During the hybridization process, when CNC was added to the CNT mixture and ensured a proper mixing, shear viscosity increased at a high rate, as depicted in Figure 1a. This increase in viscosity was also attributed to the rise in solid network formation [46]. Furthermore, an increase in viscosity was apparent by varying the CNC weight ratio between 0.4 up to 4.0 wt.% and at a constant CNT

weight ratio of 0.8 wt.%. This behavior was anticipated [45] because it was shown that the dense CNC rods promoted solid-like behavior as CNC concertation increased.

To gain further insight into the hybrid nature of the ink, the CNT to CNC ratio was fixed at 1:1, and three different concentrations (0.1:0.1, 0.5:0.5, and 0.8:0.8) were tested for their shear viscosities at a fixed angular viscosity of 0.1 rad/s as shown in Figure 1b. There was a sharp rise in the shear viscosity of CNT/CNC ink with the weight ratio of 0.8:0.8 wt.%:wt.% (total concertation of 1.6 wt.%). From an experimental point of view, inks with viscosities lower than that of CNT/CNC ink with a weight ratio of 0.5:0.5 wt.%:wt.% were not applicable on the surface of composites, probably due to inadequate network formation.

Storage (G′) and loss (G′′) moduli of CNT/CNC inks with weight ratios of 0.5:0.5 and 0.8:0.8 were evaluated at an angular frequency between 0.1 and 100 rad/sec. As shown in Figure 1c, for both inks, G′ and G′′ behaved similarly under the same frequency range. This reflects the solid-like nature of the inks [47]. G′ of both inks increased as angular frequency increased, which is a characteristic property of CNT and CNC dispersions [43,44,47–49]. Furthermore, at low frequency, it is clear that the solid-like nature of the CNT/CNC ink increased as the concentration increased; G′ of 0.8:0.8 ink, 44 Pa, was higher than that of 0.5:0.5 ink, as 20 Pa. Similar behavior has been reported for CNT-based polymeric dispersions [47,48]. G′′ behaved differently than that of G′ under the same frequency range. For small angular frequencies, 0-1 rad/sec, G′′, for both inks, decreased. As frequency increased beyond 1 rad/sec, G′′ started to increase. This behavior may suggest that at a low angular frequency range (0.1-1 rad/s) the inks showed a decent rise in elastic behavior compared with a higher frequency range (1-100 rad/s).

Shear viscosity was compared with complex viscosity for CNT/CNC ink with a weight ratio of 0.5:0.5 (wt.%:wt.%). Complex viscosity was measured as the following. Briefly, an amplitude

sweep test was carried out first to determine the linear region of the solution and then followed by a frequency sweep test at an angular frequency between 0.1 and 100 rad/sec. As shown in Figure 1d, complex viscosity results in a higher value, suggesting that CNT/CNC inks did not follow the Cox-Merz rule. Cox-Merz empirical rule is only expected to apply for CNC and CNT-based solutions of a very low concentration [43,50].

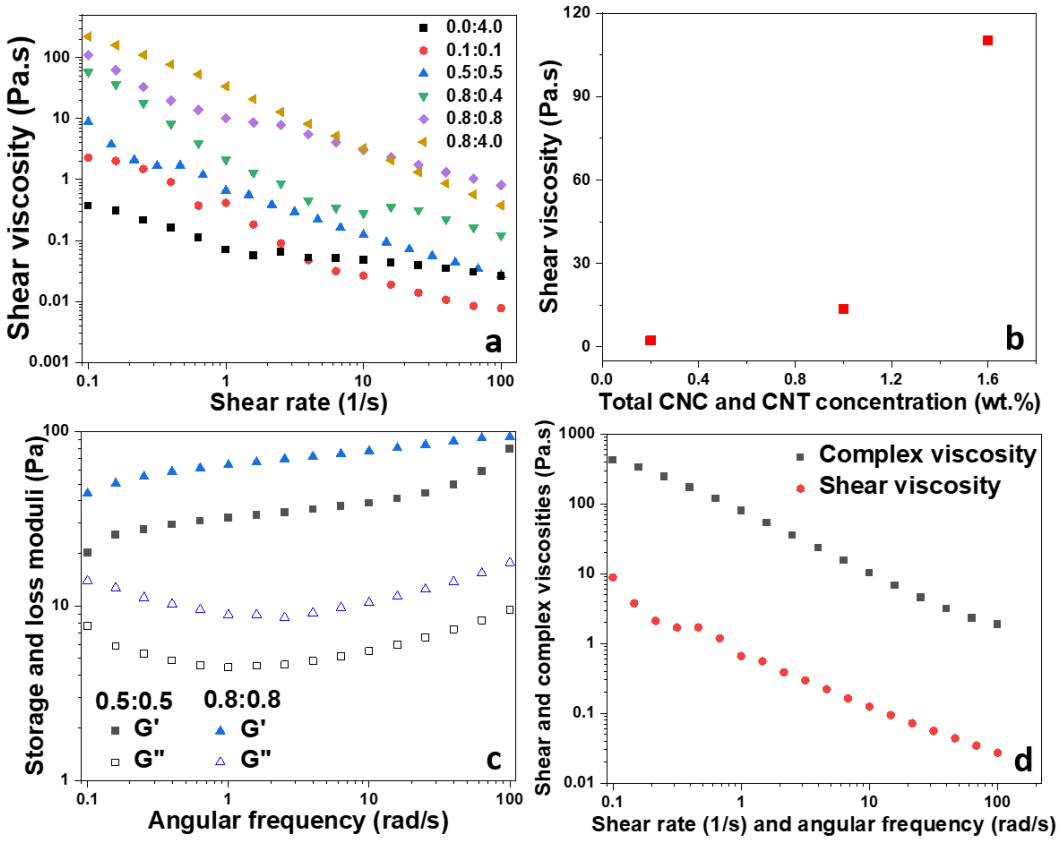

Figure 1: a) Shear viscosity as a function of shear rate for different CNT/CNC ink compositions, b) shear viscosity as a function of total CNT and CNC concentration by fixing CNT-to-CNC ratio at 1:1 (angular frequency of 0.1 rad/s), c) storage (G´) and loss (G´´) moduli as a function of angular frequency for 0.5:0.5 and 0.8:0.8 inks, and d) comparison between shear and complex viscosities for 0.5:0.5 ink.

3.2.Morphology of CNT/CNC composite sensor

Figure 2 demonstrates the micrographs of CNT/CNC strain sensors at different compositions where various CNT and CNC were mixed. Since bright spots in CNT buckypapers were attributed to the presence of a surfactant or foreign particles [51,52], here, the observed bright spots were

attributed to an excess of CNCs. CNT/CNC@0.5:0.5 concentrations presented the least of these spots, suggesting that CNCs were just adequately dispersed along the individual CNT, as shown in Figure 2a. When the weight ratio of CNTs was fixed at 0.8 wt.%, and the CNC content systemically increased from 0.4 to 4.0 (the concentrations of CNCs increased from 0.4 up to 4.0 wt.% as ten times higher), these spots' frequency was higher compared to lower compositions. The shape of these spots transitioned depending on the CNC composition, as depicted in Figure 2b where CNT/CNC@0.8:0.4 showed mostly bright single spots. As the CNC content increased these spots became linear because they were associated with the length of the curvy CNTs, as shown in Figure 2c-d. It is worth mentioning that since an earlier study [43] reported aqueous suspensions of CNC of high concentrations (as high as 20 wt.%), the increase trend in the bright spots was correlated with increase of CNC content which separated CNTs.

The surface of the sensors is of porous structure which depends on the CNC composition. The increase in CNC composition decreased the pores' frequency and apparent sizes. Plain CNT buckypapers were reported to have a porous structure too [53,54]. Also, with the increase of CNC content, it is clear that CNT entanglement and bundles tend to decrease, as shown in Figure 2b-d. This finding suggests that CNCs are highly effective in separating CNTs even after being applied and dried from an aqueous medium on the composite surface.

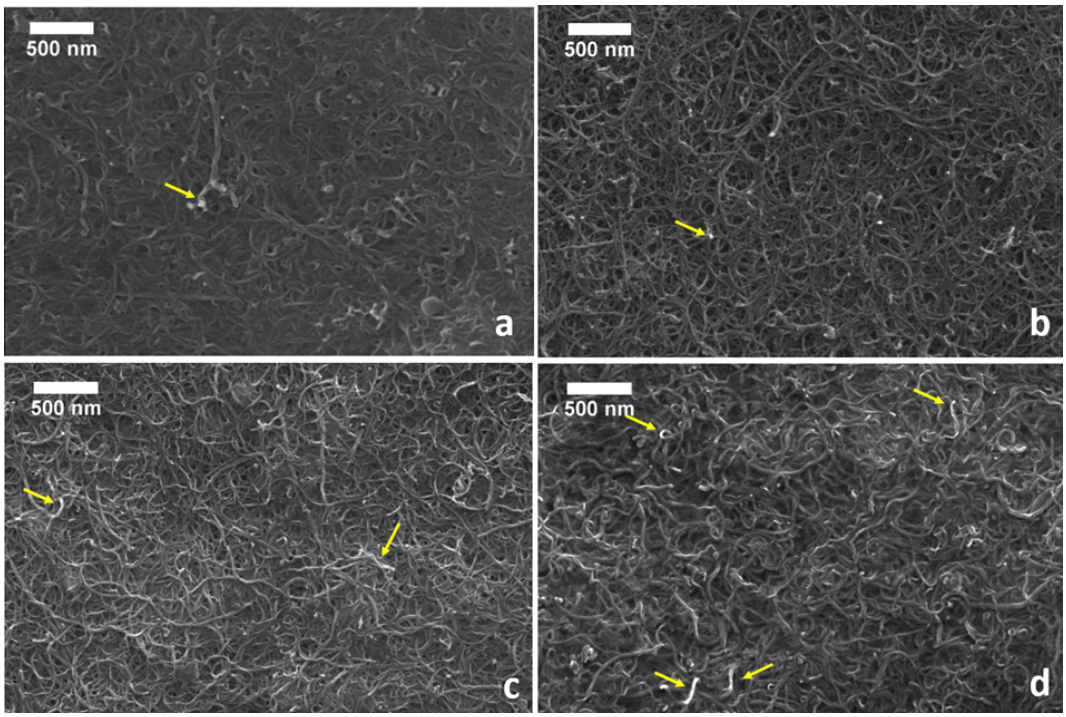

Figure 2: Surface morphology of developed strain sensors at different CNT/CNC compositions: a) 0.5:0.5, b) 0.8:0.4, c) 0.8:0.8, and d) 0.8:4.0. (yellow arrows show bright regions which were attributed to CNCs)

3.3.Electromechanical analysis

Conductive paths formed by CNTs can be categorized into two types: i) overlapping contacts and ii) in-plane contacts [55]. Overlapping contacts encompass all possible tunneling junctions between two CNTs; however, expect tip-to-tip contacts, which belong to the in-plane contacts. Previously, it was demonstrated that CNCs attach to the sidewall of an MWCNT [19,22]. By considering the large aspect ratio of CNT (length to diameter ratio, which is more significant than 650 in this study), it can be assumed that CNCs are less likely to attach to the tips of a CNT. As a result, it was concluded that the presence of CNCs alters the number of overlapping contacts without disturbing in-plane contacts, and CNCs affect the resistance of the CNT/CNC hybrid network (notice not the intrinsic resistance of individual CNT) by altering the tunneling distance.

The potential of the developed CNT/CNC piezoresistive strain sensors was first studied for their electrical properties and stabilities in the unloading state where no strain or force was applied.

First, after subjecting the sensors to different voltages ranging from -10 to 10 V, current-voltage curves were plotted. As shown in Figure 3a, all the developed sensors showed linear behavior; ohmic behavior. This desired behavior reflects the sensors' ability to resist constantly when under a wide range of voltages, which is a crucial property for a strain sensor. The initial resistance of CNT/CNC@0.8:4.0, 310 ohms, the sensor was almost threefold larger than CNT/CNC@0.8:0.4 and CNT/CNC@0.8:0.8 with initial resistances of 112 and 108 ohms, respectively. This was attributed to the ability of CNCs to physically decrease the number of available tunneling junctions and increase tunneling distance. This claim is also supported by the morphology analysis carried out in the previous section in a qualitative fashion, and it will be further validated when the results of modeling analyses are explained.

The stability of sensors was evaluated by applying a constant voltage, 2.1 V as demonstrated in Figure S2. Change in resistance as a function of time was plotted for the developed sensors. CNT/CNC@0.5:0.5 sensors showed negligible change in resistance, while CNT/CNC@0.8:4.0 showed the most significant change in resistance over the same period. At room temperature, CNT/CNC@0.5:0.5 reached almost immediate stability. However, CNT/CNC@0.8:4.0 reached near stability only after 200 seconds had passed.

It is noted that the recorded change in resistance was negative, demonstrating that the sensors' conductivity increased after the voltage difference application. Such an increase in conductivity after applying voltage difference has been reported for CNT-based nanocomposite sensors [56]. The rise in temperature in an individual CNT, as a result of Joule heating, when a voltage is applied, supplies sufficient energy for electrons to tunnel between adjacent CNT particles [57]. Also, previous studies showed that CNC can retain moisture in its crystallinity [35] and CNC has lower thermal conductivity compared with CNT [58,59]. Therefore, it was concluded that, as a

result of Joule heating, the electrical stability of CNT/CNC sensors is heavily dependent on the content of CNCs. It was, thus, thought that due to the high content of CNCs in CNT/CNC@0.8:4.0 sensor electrical stability took longer time to stabilize because of (i) relatively low number of CNT contacts, (ii) relatively high retained moisture content within crestline structure of CNC, and (iii) low thermal conductivity. All combined, may resulted in delaying the transportation of electrons during Joule heating.

To gain more insights on the effect of moisture content on stability of the sensors, the stability of CNT/CNC@0.5:0.5 and CNT/CNC@0.8:4.0 was tested at elevated temperatures. Figure 3b shows that changes in resistances at room temperature and 40 $^{\circ}$C for CNT/CNC@0.5:0.5 sensor were almost identical. Although the initial resistance dropped when the temperature was elevated (see Figure S3), the rate of change in resistance was the same. The stability of CNT/CNC@0.8:4.0 was faster than when the change in resistance was measured at room temperature. This shows that CNT/CNC sensors' stability might be dependent on moisture content which is dependent on CNC content. More studies are needed, however, to unravel the effect of moisture retention and thermal conductivity on CNT/CNC sensors.

The following comparison with plain CNT-based samples was carried out. Adopting a 4-point measuring configuration using Keithley, change in resistance for pure CNT buckypaper, CNT epoxy nanocomposite (0.5 wt.%), and CNT/CNC@0.5:0.5 were measured over a period of time under the exact conditions. Results are demonstrated in Figure S4. It was evident that CNT/CNC-based sample showed better electrical stability compared with the other two CNT-based samples. Overall, all CNT/CNC-based sensors showed minor changes in resistance, less than 0.6%, for up to 300 seconds.

Since a CNC is attached to a CNT at its defect points, mainly sidewalls, not the tip of the CNT (*e.g.,* oxygen presence), and not by creating a new defect nor by altering the nature of the outermost layer of the CNT, it is proposed that CNC does not add additional elastic scattering to electrons when a voltage difference is applied to an individual CNT. Therefore, under applied voltage difference, electrons are only elastically scattered due to the existing defects [60] despite the attraction between CNCs and the CNT. It was concluded that CNC provides electrical stability when a CNT is subjected to voltage differences. Also, the CNT to CNC ratio plays a role in determining the degree of stability.

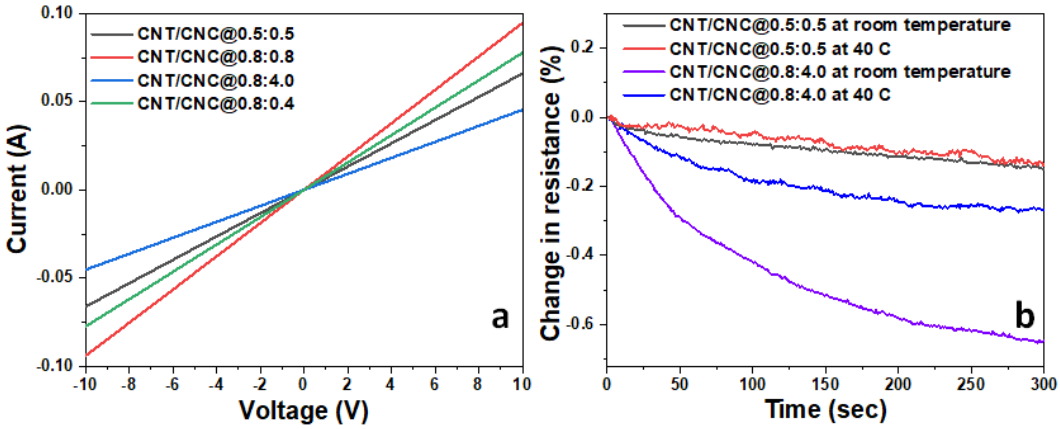

Figure 3: a) Current-voltage curves for the developed sensors and b) change in sheet resistance in unloading state as a function of CNC under different temperatures.

Mechanical properties of GFRP were determined by conducting a tensile test following the ASTM D3039 standard. Extensometer was used to measure strains accurately up to around 1.35%. After the extensometer's removal, the test continued until fracture. The tensile strain graph is shown in Figure 4a, and other properties are summarized in Table S1. It was determined that the elastic region of the vacuum-infused GFRP composite ends at a strain of 0.6%.

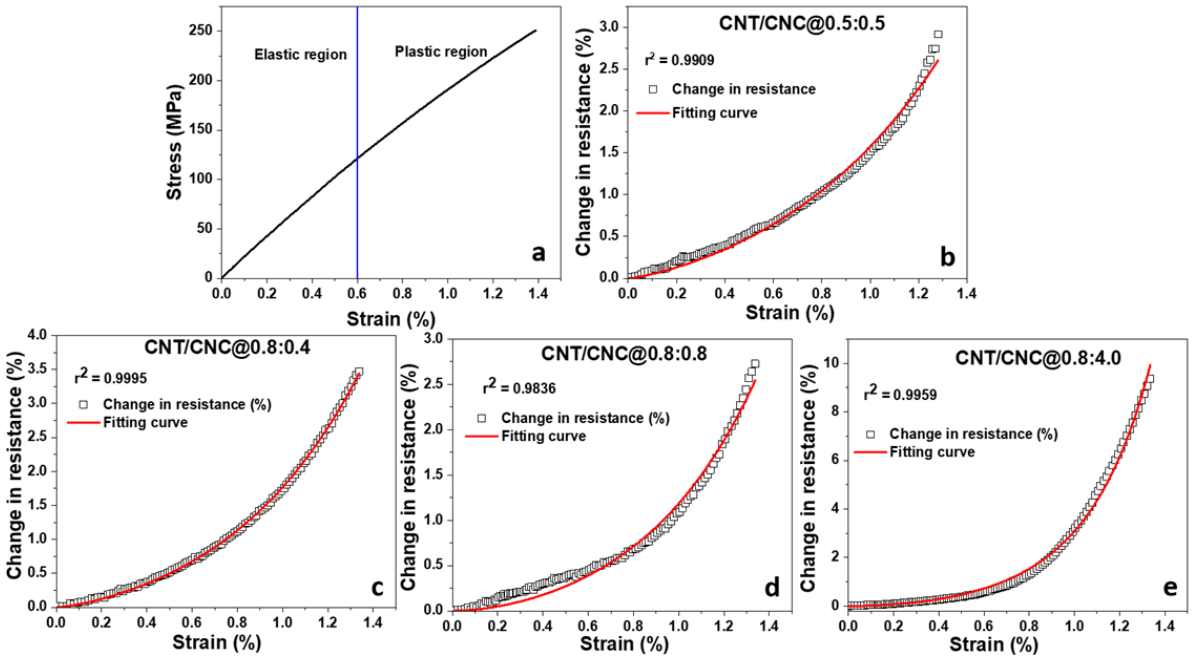

Figure 4: a) Stress-strain graph, and experimental and theoretical tensile piezoresistive behavior of b) CNT/CNC@0.5:0.5, c) CNT/CNC@0.8:0.4, d) CNT/CNC@0.8:0.8, and e) CNT/CNC@0.8:4.0.

Change in resistance was measured by subjecting CNT/CNC-coated samples to a tensile test following the same ASTM standard, D3039, used earlier to determine the mechanical properties. Similarly, the extensometer was removed after the strain reached around 1.35%. That said, to show all changes in the strain sensor, changes in resistance as a function of time for the CNT/CNC@0.5:0.5 sensors were recorded until fracture, as shown in Figure S5. To determine the piezoresistive behavior of the sensors, the resistance was measured using a silver-pasted two-probe configuration using the Keithley source meter, and the change in resistance was calculated using Equation 9

$$\frac{\Delta R}{R_0} \times 100 = \frac{R_i - R_0}{R_0} \times 100 \qquad \text{Equation (9)}$$

where R_i and R_0 are instantaneous and initial resistances, respectively. Initial resistance is the resistance measured before the application of a force.

The gauge factor and sensitivity of the sensors were calculated based on Equation 10

$$\text{Gauge Factor} = \frac{\Delta R}{R_0 \varepsilon} \qquad \text{Equation (10)}$$

Four sensors, CNT/CNC@0.5:0.5, CNT/CNC@0.8:0.4, CNT/CNC@0.8:0.8, and CNT/CNC@0.8:4.0, at different CNT/CNC compositions were selected to be tested for their tensile piezoresistive properties. The piezoresistive behavior was studied under both elastic and plastic deformations. Depending on the CNT/CNC composition, different responses were observed in Figure 4b-e. CNT/CNC@0.5:0.5 and CNT/CNC@0.8:0.8 sensors captured and matched the elastic region of the composite, demonstrating the feasibility of coating application. The linearity of the sensors, r^2, under the elastic region was high, as tabulated in Table 4. CNT/CNC@0.5:0.5 showed a higher gauge factor than CNT/CNC@0.8:0.8; 1.0 and 0.7, respectively. The difference between the sensitivity of these two sensors was attributed to the composition of CNT/CNC in CNT/CNC@0.5:0.5, which is close to the rheological percolation threshold (see Figure 1b). Similar results were identified in the literature, and it was shown that sensitivity was higher at percolation load, and as the CNT loading increased sensitivity dropped [32,61,62].

When the CNT ratio was fixed at 0.8 wt.%, and the CNC ratio was increased from 0.4 to 4.0 wt.%, CNT/CNC@0.8:0.4, CNT/CNC@0.8:0.8, and CNT/CNC@0.8:4.0 showed distinct piezoresistive behaviors. Initially, CNT/CNC@0.8:0.4 and CNT/CNC@0.8:4.0 could not capture the entire elastic region of the composite, as shown in Figure 4c and Figure 4e. Only to around 0.30% strain high linearity was maintained. Also, as the CNC composition increased, gauge factors for the elastic region decreased from 0.9 to 0.5. However, an inverse pattern was seen for the calculated maximum gauge factor in the plastic region (1.20-1.35% strain). CNT/CNC@0.8:4.0 had the

highest gauge factor of 22.2. In literature, at least for the elastic region of CNT nanocomposites, it has been established that the sensitivity increases as CNT load decreases [63] which is the opposite trend we observed as the CNT amount decreased by increasing the CNC loading. This was reconciled as follows.

The conductive network paths in the presence of a high load of CNC subjected to an external strain was thought to mimic that of aligned CNT conductive network paths. To demonstrate, when a plain aligned CNT conductive network is subjected to a strain in the direction of the alignment, the increase in tunneling distance is lower than when the aligned CNT network is subjected to a strain in the transverse direction [64], which leads to lower gauge factors in the alignment direction. Although, in our case, the CNTs were randomly aligned, the dominant contribution in a change in tunneling distance in the network of CNT in the presence of high loads of CNC (*e.g.* CNT/CNC@0.8:4.0) was mainly limited to in-plane tunneling. In other words, in-plane contacts that are in the direction of strain (relative tunneling distance of in-plane contacts that are in transverse direction with the applied strain would decrease in instead) shall exhibit the same change in tunneling distance as those of aligned CNT contacts. Hence, in-plane tunneling becomes dominant at high loads of CNCs (*e.g.* CNT/CNC@0.8:4.0). This understanding could be quantified by Equation 11 [65]. The equation describes the influence on the gauge factor as a result of geometrical changes and changes in resistance due to changes in tunneling resistance.

$$\text{Gauge Factor} = (1 + 2v) + \frac{\Delta R}{R_0 \varepsilon} \qquad \text{Equation (11)}$$

The geometrical gauge factor was calculated to be 1.62 (for Poisson's ratio of 0.31), which suggests that the piezoresistive change of CNT/CNC sensors seen in the elastic region (0-0.6%) could be attributed to mainly geometrical changes. In plastic region the piezoresistive change could be

attributed to a pronounced change in tunneling distance amongst CNT particles [32]. As can be observed in Table 4, as CNC content increased gauge factors in plastic region increased. Since a changes in piezoresistive in plastic region was thought to be due to a change in tunneling distance, the increase in gauge factors with increase of CNC content could be attributed to the imbalances in CNT network [32,66]. But since in our case CNTs are not dispersed into a typical polymer matrix, these imbalances were thought to be due to difference between CNT contact types formed as a result of different CNC content; overlapping contacts which may be dominant at low load of CNCs and in-plane contacts which may be dominant at high load of CNCs.

The fitting procedure after applying Equation 8 was performed and resulted in a good match between theoretical and experimental comparison. Using Equation 8, the average initial tunneling distance, t_0, for the developed sensors was determined, and the results are summarized in Table 4. It is important to note that the modeling effort herein emphasizes the relation between the approximated average initial tunneling distance and CNC content rather than the actual or absolute values of tunneling distance. Table 4 shows that when the CNT content was constant (0.8 wt.%), approximated tunneling distance for 7 for CNT/CNC@0.8:0.4 and CNT/CNC@0.8:4.0 increased from 0.4 up to 0.7, respectively. Since the CNCs tend to attach to sidewalls of CNTs rather than to their tips, the increase in average tunneling distance was regarded as an increase in overlapping contacts, while in-plane tunneling distance remained unchanged. We concluded that the tunneling distance is a function of CNC content.

Table 4: Properties and characteristics of the CNT/CNC strain sensors.

Given name	Gauge factor*	Max. gauge factor*	B**

	0-0.30% strain [r^2]	0-0.60% strain [r^2]	1.20-1.35% strain [r^2]	Average tunneling distance, t_0, (nm)**	
CNT/CNC@0.5:0.5	1.0 [0.997]	1.0 [0.997]	7.7 [0.975]	0.4	1.3
CNT/CNC@0.8:0.4	0.9 [0.991]	-	6.3 [0.998]	0.4	1.4
CNT/CNC@0.8:0.8	0.7 [0.996]	0.7 [0.996]	6.4 [0.993]	0.3	1.8
CNT/CNC@0.8:4.0	0.5 [0.998]	-	22.2 [0.999]	0.7	1.9

* gauge factors were calculated for linear regions,

** tunneling distance and B were best fitting results based on Equation 8.

The value of B also increased as the CNC content increased, which suggests that the nonlinear relation between average tunneling distance and strain increases at a raise of the CNC content. To gain further insights, change in tunneling distance and tunneling distance as function of strain was plotted using Equation 4. Figure 5a shows that at any strain value (below 1%), at the lower CNC content, the change in tunneling is achieved higher. This relation suggests that the movements of CNTs are impaired by the CNCs. This impairment could be attributed to CNCs occupying the available tunneling junctions on a CNT. With the assumption that CNCs tend to attach to the side of walls of a CNT rather than to its ends, B can be interpreted as an indirect indication of CNT-CNT interaction under strain in the presence of CNCs. Hence, higher B values for elastic regions yield a low sensitivity under strain; for example, CNT/CNC@0.8:4.0 has the lowest gauge factor (between 0-0.30% strain). In plastic regions, when permanent deformation occurs, B and the initial average tunneling distance determine the sensor's sensitivity. For example, although tunneling distance in CNT/CNC@0.8:4.0 has a lower change in compared with other sensors' tunneling

distances, the approximated initial average tunneling distance, 0.7 nm, was closer to the cutoff distance (1.40-1.80 nm) [14,67] in comparison with the tunneling distances of the other sensors as shown in Figure 5b.

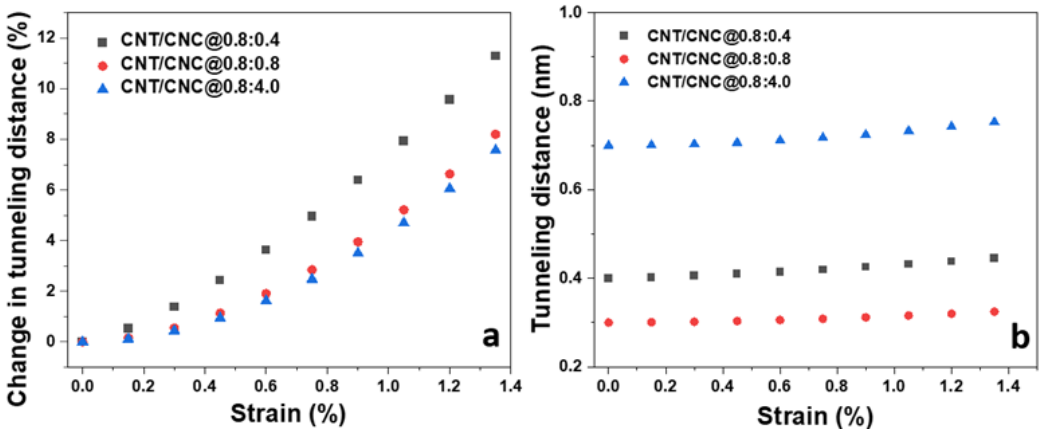

Figure 5: a) Change in tunneling distance and b) tunneling distance as a function of strains at various CNC compositions.

Based on the previous findings and premises developed in this work and the accumulated knowledge from the literature, it is concluded that the effect of highly loaded CNCs on the CNTs conductive paths diminishes the required routes for electron transfer, as demonstrated in Figure 6. Hence, it is shown that at low loads of CNCs, both in-plane and overlapping contacts are responsible for electron tunneling. At high loads of CNCs, however, mainly in-plane contacts are responsible for electron tunneling. Therefore, an applied strain invokes higher changes in average tunneling distance in a medium where CNC loads are lower than in a medium where CNC loads are high. It is worth reporting that the good reproducibility of the results was emphasized through the average values of gauge factors, B values, and the initial tunneling distances of three identical sensors for each of the developed sensors (See Table S2).

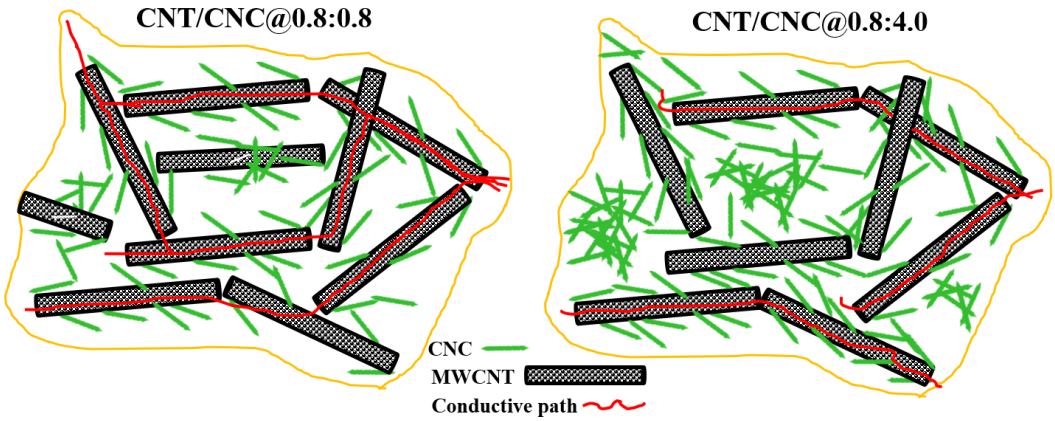

Figure 6: Effect of CNCs, at low and high loads, on the type of CNT contacts and conductive paths.

To demonstrate the feasibility and durability of the CNT/CNC sensors as an application for structural health monitoring systems, a reliable performance test was carried out in elastic region (at 0.60% strain). CNT/CNC@0.8:0.8 was subjected to 250 tensile cycles with a crosshead speed of 6 mm/min. As demonstrated in Figure 7, the negative piezoresistive behavior of the sensor, which was previously seen in [68,69], was attributed to three main reasons: i) permanent changes in the CNT conductive network [69], ii) Poisson effect [12,70], and iii) mechanical hysteresis [70]. Our attribution to the decrease in resistance during cyclic loading, however, could be related mainly to the continuous reconstruction of CNT conductive pathways. As discussed in supporting information, although mechanical hysteresis has an effect on cyclic loading, its effect was not continuously dominant after the first few cycles (see Figure S6 for more information). To better exploit this phenomenon in strain sensing for practical applications, the mechanism of this behavior is yet to be fully understood which requires further investigation. Nonetheless, after 250 cycles the CNT/CNC composite on the surface of GFRP composite remained intact demonstrating the feasibility of coating CNT/CNC on surface of composites and the durability of the coated layer. Further in-depth discussion and comparison between sensors' performance are provided in supporting information.

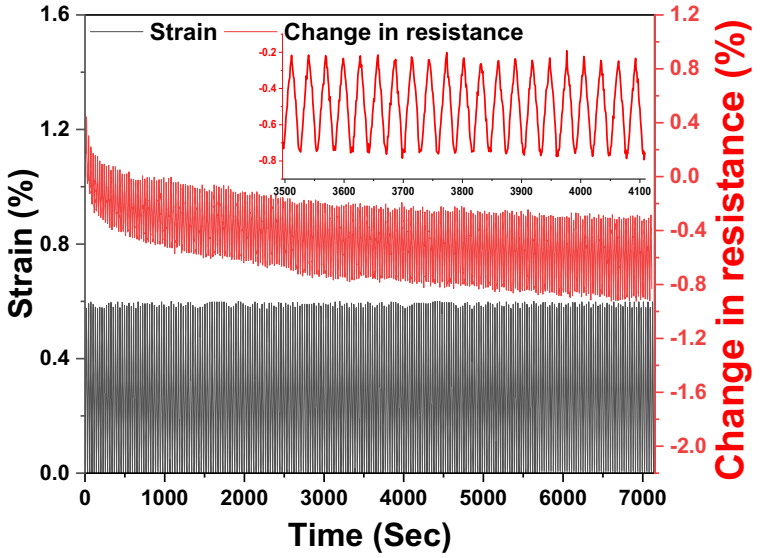

Figure 7: Piezoresistive behavior as a function of time for a total of 250 cycles for CNT/CNC@0.8:0.8 at a strain of 0.60%. Inset figure shows enlarged portion of change in resistance at time interval between 3500 and 4120 second.

4. Conclusion

This work demonstrated a practical approach to functionalize CNT/CNC composite as strain sensors prepared from aqueous inks. First, the rheological behavior of CNT/CNC inks was studied, and then the morphological and electrical properties were reported for the CNT/CNC sensors. Morphological analysis showed that CNCs effectively separate CNTs bundles in a non-aqueous medium. CNT/CNC sensors showed ohmic behavior and electrical stability. Electromechanical results showed that the behavior and sensitivities of the sensors, at small and large strains, were depended on the initial composition of CNCs. Gauge factor as high as 1.0 was calculated for the elastic region for CNT/CNC composite with composition of 0.5:0.5 (wt.%:wt.%), and a gauge factor of 22.2 was calculated for the plastic region for CNT/CNC composite with composition of 0.8:4.0 (wt.%:wt.%). It was demonstrated that CNC particles could control the type of contacts between CNTs and their average tunneling distance. The modified analytical model further supported the previous finding; by increasing the CNC content the average tunneling distance

between CNTs increased. It is concluded that the piezoresistive behavior of the CNT/CNC composite sensor and average tunneling distance is controllable by manipulating the initial composition of the CNT/CNC inks, and a proposed mechanism was provided. Also, applying a binder-free and environmentally friendly sustainable aqueous ink on a surface of a composite was demonstrated to be an effective and practical approach for strain sensing.

CRediT authorship contribution statement

Adel Alrai: Investigation, Data curation, Writing – original draft, Writing – review & editing, Visualization. **Ersin Beyhan**: Investigation, Data curation, Writing – review & editing. **Elif Ozden-Yenigün**: Formal analysis, Writing – review & editing. **Amir Asadi**: Methodology, Resources. **Hülya Cebeci**: Conceptualization, Methodology, Writing – review & editing, Supervision, Project administration, Funding acquisition.

Declaration of competing interest

The authors declare that they have no known competing financial interests or personal relationships that could have appeared to influence the work reported in this paper.

Acknowledgments

This work was financially supported by Istanbul Technical University Aerospace Research Center. The authors would like to thank Suat Ebil and Yunus Emre Bozkurt for their help carrying out rheology tests. The authors would like to thank Erdem Kilicaslan for his help obtaining scanning electron microscopy images.

Reference

[1] G. Monastyreckis, A. Stepura, Y. Soyka, H. Maltanava, S.K. Poznyak, M. Omastová, A. Aniskevich, D. Zeleniakiene, Strain Sensing Coatings for Large Composite Structures Based on 2D MXene Nanoparticles, Sensors. 21 (2021) 2378. https://doi.org/10.3390/s21072378.

[2] M. Wang, N. Li, G.-D. Wang, S.W. Lu, Q.D. Zhao, X.L. Liu, High-sensitive flexural sensors for health monitoring of composite materials using embedded carbon nanotube (CNT) buckypaper, Composite Structures. 261 (2021) 113280. https://doi.org/10.1016/j.compstruct.2020.113280.

[3] A.Y. Fedorov, N.A. Kosheleva, V.P. Matveenko, G.S. Serovaev, Strain measurement and stress analysis in the vicinity of a fiber Bragg grating sensor embedded in a composite material, Composite Structures. 239 (2020) 111844. https://doi.org/10.1016/j.compstruct.2019.111844.

[4] D. Kinet, P. Mégret, K.W. Goossen, L. Qiu, D. Heider, C. Caucheteur, Fiber Bragg Grating Sensors toward Structural Health Monitoring in Composite Materials: Challenges and Solutions, Sensors. 14 (2014) 7394–7419. https://doi.org/10.3390/s140407394.

[5] M. Reghat, A. Mirabedini, A.M. Tan, Y. Weizman, P. Middendorf, R. Bjekovic, L. Hyde, D. Antiohos, N. Hameed, F.K. Fuss, B. Fox, Graphene as a piezo-resistive coating to enable

strain monitoring in glass fiber composites, Composites Science and Technology. 211 (2021) 108842. https://doi.org/10.1016/j.compscitech.2021.108842.
[6] P. Zarrintaj, M. Jouyandeh, M.R. Ganjali, B.S. Hadavand, M. Mozafari, S.S. Sheiko, M. Vatankhah-Varnoosfaderani, T.J. Gutiérrez, M.R. Saeb, Thermo-sensitive polymers in medicine: A review, European Polymer Journal. 117 (2019) 402–423. https://doi.org/10.1016/j.eurpolymj.2019.05.024.
[7] X. Zhang, D. Xiang, W. Zhu, Y. Zheng, E. Harkin-Jones, P. Wang, C. Zhao, H. Li, B. Wang, Y. Li, Flexible and high-performance piezoresistive strain sensors based on carbon nanoparticles@polyurethane sponges, Composites Science and Technology. 200 (2020) 108437. https://doi.org/10.1016/j.compscitech.2020.108437.
[8] L. Paleari, M. Bragaglia, F. Fabbrocino, F. Nanni, Structural Monitoring of Glass Fiber/Epoxy Laminates by Means of Carbon Nanotubes and Carbon Black Self-Monitoring Plies, Nanomaterials. 11 (2021) 1543. https://doi.org/10.3390/nano11061543.
[9] H. Yazdani, K. Hatami, E. Khosravi, K. Harper, B.P. Grady, Strain-sensitive conductivity of carbon black-filled PVC composites subjected to cyclic loading, Carbon. 79 (2014) 393–405. https://doi.org/10.1016/j.carbon.2014.07.082.
[10] B. Hao, Q. Ma, S. Yang, E. Mäder, P.-C. Ma, Comparative study on monitoring structural damage in fiber-reinforced polymers using glass fibers with carbon nanotubes and graphene coating, Composites Science and Technology. 129 (2016) 38–45. https://doi.org/10.1016/j.compscitech.2016.04.012.
[11] S. Datta, R.K. Neerukatti, A. Chattopadhyay, Buckypaper embedded self-sensing composite for real-time fatigue damage diagnosis and prognosis, Carbon. 139 (2018) 353–360. https://doi.org/10.1016/j.carbon.2018.06.059.
[12] S. Luo, W. Obitayo, T. Liu, SWCNT-thin-film-enabled fiber sensors for lifelong structural health monitoring of polymeric composites - From manufacturing to utilization to failure, Carbon. 76 (2014) 321–329. https://doi.org/10.1016/j.carbon.2014.04.083.
[13] M.K. Njuguna, C. Yan, N. Hu, J.M. Bell, P.K.D.V. Yarlagadda, Sandwiched carbon nanotube film as strain sensor, Composites Part B: Engineering. 43 (2012) 2711–2717. https://doi.org/10.1016/j.compositesb.2012.04.022.
[14] B. De Vivo, P. Lamberti, G. Spinelli, V. Tucci, L. Vertuccio, V. Vittoria, Simulation and experimental characterization of polymer/carbon nanotubes composites for strain sensor applications, Journal of Applied Physics. 116 (2014) 054307. https://doi.org/10.1063/1.4892098.
[15] N. Hu, Y. Karube, M. Arai, T. Watanabe, C. Yan, Y. Li, Y. Liu, H. Fukunaga, Investigation on sensitivity of a polymer/carbon nanotube composite strain sensor, Carbon. 48 (2010) 680–687. https://doi.org/10.1016/j.carbon.2009.10.012.
[16] N. Hu, Z. Masuda, G. Yamamoto, H. Fukunaga, T. Hashida, J. Qiu, Effect of fabrication process on electrical properties of polymer/multi-wall carbon nanotube nanocomposites, Composites Part A: Applied Science and Manufacturing. 39 (2008) 893–903. https://doi.org/10.1016/j.compositesa.2008.01.002.
[17] S. Wang, X. Zhang, X. Wu, C. Lu, Tailoring percolating conductive networks of natural rubber composites for flexible strain sensors via a cellulose nanocrystal templated assembly, Soft Matter. 12 (2016) 845–852. https://doi.org/10.1039/C5SM01958C.
[18] X. Liu, G. Su, Q. Guo, C. Lu, T. Zhou, C. Zhou, X. Zhang, Hierarchically Structured Self-Healing Sensors with Tunable Positive/Negative Piezoresistivity, Adv. Funct. Mater. 28 (2018) 1706658. https://doi.org/10.1002/adfm.201706658.

[19] S. Shariatnia, A.V. Kumar, O. Kaynan, A. Asadi, Hybrid Cellulose Nanocrystal-Bonded Carbon Nanotubes/Carbon Fiber Polymer Composites for Structural Applications, ACS Appl. Nano Mater. 3 (2020) 5421–5436. https://doi.org/10.1021/acsanm.0c00785.
[20] I. Ibanez Labiano, D. Arslan, E. Ozden Yenigun, A. Asadi, H. Cebeci, A. Alomainy, Screen Printing Carbon Nanotubes Textiles Antennas for Smart Wearables, Sensors. 21 (2021) 4934. https://doi.org/10.3390/s21144934.
[21] Q. Yan, W. Xie, M. Zhou, H. Fu, An ultrasensitive and highly compressive piezoresistive sensor based on a biopolyol-reinforced polyurethane sponge coated with silver nanoparticles and carbon nanotubes/cellulose nanocrystals, J. Mater. Chem. C. 8 (2020) 16603–16614. https://doi.org/10.1039/D0TC04141F.
[22] A. Hajian, S.B. Lindström, T. Pettersson, M.M. Hamedi, L. Wågberg, Understanding the Dispersive Action of Nanocellulose for Carbon Nanomaterials, Nano Lett. 17 (2017) 1439–1447. https://doi.org/10.1021/acs.nanolett.6b04405.
[23] J.-B. Mougel, C. Adda, P. Bertoncini, I. Capron, B. Cathala, O. Chauvet, Highly Efficient and Predictable Noncovalent Dispersion of Single-Walled and Multi-Walled Carbon Nanotubes by Cellulose Nanocrystals, J. Phys. Chem. C. 120 (2016) 22694–22701. https://doi.org/10.1021/acs.jpcc.6b07289.
[24] M. Aramfard, O. Kaynan, E. Hosseini, M. Zakertabrizi, L.M. Pérez, A. Asadi, Aqueous Dispersion of Carbon Nanomaterials with Cellulose Nanocrystals: An Investigation of Molecular Interactions, Small. n/a (n.d.) 2202216. https://doi.org/10.1002/smll.202202216.
[25] F. Panozzo, M. Zappalorto, M. Quaresimin, Analytical model for the prediction of the piezoresistive behavior of CNT modified polymers, Composites Part B: Engineering. 109 (2017) 53–63. https://doi.org/10.1016/j.compositesb.2016.10.034.
[26] Z.-H. Tang, Y.-Q. Li, P. Huang, H. Wang, N. Hu, S.-Y. Fu, Comprehensive evaluation of the piezoresistive behavior of carbon nanotube-based composite strain sensors, Composites Science and Technology. 208 (2021) 108761. https://doi.org/10.1016/j.compscitech.2021.108761.
[27] M.C. Andrews, R.J. Day, X. Hu, R.J. Young, Dependence of fibre strain on orientation angle for off-axis fibres in composites, J Mater Sci Lett. 11 (1992) 1344–1346. https://doi.org/10.1007/BF00729357.
[28] W. Zheng, J. Xie, J. Zhang, C. Tang, Z. Zhao, Influence of Polymethylsilsesquioxane Content to the Thermal Stability of Meta-Aramid Fiber Insulation Paper, Materials. 11 (2018) 2317. https://doi.org/10.3390/ma11112317.
[29] S. Pavlopoulou, S.S. Roy, M. Gautam, L. Bradshaw, P. Potluri, Numerical and Experimental Investigation of the Hydrostatic Performance of Fibre Reinforced Tubes, Appl Compos Mater. 24 (2017) 417–448. https://doi.org/10.1007/s10443-016-9563-7.
[30] M. Park, H. Kim, J.P. Youngblood, Strain-dependent electrical resistance of multi-walled carbon nanotube/polymer composite films, Nanotechnology. 19 (2008) 055705. https://doi.org/10.1088/0957-4484/19/05/055705.
[31] L. Onsager, The Effects of Shape on the Interaction of Colloidal Particles, Annals of the New York Academy of Sciences. 51 (1949) 627–659. https://doi.org/10.1111/j.1749-6632.1949.tb27296.x.
[32] M.H.G. Wichmann, S.T. Buschhorn, J. Gehrmann, K. Schulte, Piezoresistive response of epoxy composites with carbon nanoparticles under tensile load, Phys. Rev. B. 80 (2009) 245437. https://doi.org/10.1103/PhysRevB.80.245437.

[33] A. Mdarhri, F. Carmona, C. Brosseau, P. Delhaes, Direct current electrical and microwave properties of polymer-multiwalled carbon nanotubes composites, Journal of Applied Physics. 103 (2008) 054303. https://doi.org/10.1063/1.2841461.
[34] T. Tanaka, E. Sano, M. Imai, K. Akiyama, Electrical conductivity of carbon-nanotube/cellulose composite paper, Journal of Applied Physics. 107 (2010) 054307. https://doi.org/10.1063/1.3319675.
[35] A. Mihranyan, A.P. Llagostera, R. Karmhag, M. Strømme, R. Ek, Moisture sorption by cellulose powders of varying crystallinity, International Journal of Pharmaceutics. 269 (2004) 433–442. https://doi.org/10.1016/j.ijpharm.2003.09.030.
[36] J.M. González-Domínguez, A. Ansón-Casaos, L. Grasa, L. Abenia, A. Salvador, E. Colom, J.E. Mesonero, J.E. García-Bordejé, A.M. Benito, W.K. Maser, Unique Properties and Behavior of Nonmercerized Type-II Cellulose Nanocrystals as Carbon Nanotube Biocompatible Dispersants, Biomacromolecules. 20 (2019) 3147–3160. https://doi.org/10.1021/acs.biomac.9b00722.
[37] I. Kalashnikova, H. Bizot, B. Cathala, I. Capron, New Pickering Emulsions Stabilized by Bacterial Cellulose Nanocrystals, Langmuir. 27 (2011) 7471–7479. https://doi.org/10.1021/la200971f.
[38] J. George, S. Sabapathi, Cellulose nanocrystals: synthesis, functional properties, and applications, Nanotechnol Sci Appl. 8 (2015) 45–54. https://doi.org/10.2147/NSA.S64386.
[39] R.M.A. Domingues, M.E. Gomes, R.L. Reis, The Potential of Cellulose Nanocrystals in Tissue Engineering Strategies, Biomacromolecules. 15 (2014) 2327–2346. https://doi.org/10.1021/bm500524s.
[40] C. Olivier, C. Moreau, P. Bertoncini, H. Bizot, O. Chauvet, B. Cathala, Cellulose Nanocrystal-Assisted Dispersion of Luminescent Single-Walled Carbon Nanotubes for Layer-by-Layer Assembled Hybrid Thin Films, Langmuir. 28 (2012) 12463–12471. https://doi.org/10.1021/la302077a.
[41] S. Onogi, T. Asada, Rheology and Rheo-Optics of Polymer Liquid Crystals, in: G. Astarita, G. Marrucci, L. Nicolais (Eds.), Rheology: Volume 1: Principles, Springer US, Boston, MA, 1980: pp. 127–147. https://doi.org/10.1007/978-1-4684-3740-9_9.
[42] U. Casado, V.L. Mucci, M.I. Aranguren, Cellulose nanocrystals suspensions: Liquid crystal anisotropy, rheology and films iridescence, Carbohydrate Polymers. 261 (2021) 117848. https://doi.org/10.1016/j.carbpol.2021.117848.
[43] C. Qiao, G. Chen, J. Zhang, J. Yao, Structure and rheological properties of cellulose nanocrystals suspension, Food Hydrocolloids. 55 (2016) 19–25. https://doi.org/10.1016/j.foodhyd.2015.11.005.
[44] M.-C. Li, Q. Wu, K. Song, S. Lee, Y. Wu, Cellulose Nanoparticles: Structure–Morphology–Rheology Relationships, ACS Sustainable Chemistry & Engineering. 3 (2015) 150407061249007. https://doi.org/10.1021/acssuschemeng.5b00144.
[45] M. Bercea, P. Navard, Shear Dynamics of Aqueous Suspensions of Cellulose Whiskers, Macromolecules. 33 (2000) 6011–6016. https://doi.org/10.1021/ma000417p.
[46] Q. Zhang, S. Rastogi, D. Chen, D. Lippits, P.J. Lemstra, Low percolation threshold in single-walled carbon nanotube/high density polyethylene composites prepared by melt processing technique, Carbon. 44 (2006) 778–785. https://doi.org/10.1016/j.carbon.2005.09.039.
[47] F. Du, R.C. Scogna, W. Zhou, S. Brand, J.E. Fischer, K.I. Winey, Nanotube Networks in Polymer Nanocomposites: Rheology and Electrical Conductivity, Macromolecules. 37 (2004) 9048–9055. https://doi.org/10.1021/ma049164g.

[48] Z. Fan, S.G. Advani, Rheology of multiwall carbon nanotube suspensions, Journal of Rheology. 51 (2007) 585–604. https://doi.org/10.1122/1.2736424.
[49] K. Chiou, S. Byun, J. Kim, J. Huang, Additive-free carbon nanotube dispersions, pastes, gels, and doughs in cresols, Proc. Natl. Acad. Sci. U.S.A. 115 (2018) 5703–5708. https://doi.org/10.1073/pnas.1800298115.
[50] K. Xiao, L. Zhang, I. Zarudi, Mechanical and rheological properties of carbon nanotube-reinforced polyethylene composites, Composites Science and Technology. 67 (2007) 177–182. https://doi.org/10.1016/j.compscitech.2006.07.027.
[51] J.L. Rigueur, S.A. Hasan, S.V. Mahajan, J.H. Dickerson, Buckypaper fabrication by liberation of electrophoretically deposited carbon nanotubes, Carbon. 48 (2010) 4090–4099. https://doi.org/10.1016/j.carbon.2010.07.016.
[52] T. Zhu, Y. Zhang, L. Luo, X. Zhao, Facile Fabrication of NiO-Decorated Double-Layer Single-Walled Carbon Nanotube Buckypaper for Glucose Detection, ACS Appl. Mater. Interfaces. 11 (2019) 10856–10861. https://doi.org/10.1021/acsami.9b00803.
[53] J. Zhang, D. Jiang, Influence of geometries of multi-walled carbon nanotubes on the pore structures of Buckypaper, Composites Part A: Applied Science and Manufacturing. 43 (2012) 469–474. https://doi.org/10.1016/j.compositesa.2011.11.016.
[54] R.L.D. Whitby, T. Fukuda, T. Maekawa, S.L. James, S.V. Mikhalovsky, Geometric control and tuneable pore size distribution of buckypaper and buckydiscs, Carbon. 46 (2008) 949–956. https://doi.org/10.1016/j.carbon.2008.02.028.
[55] T. Takeda, Y. Shindo, Y. Kuronuma, F. Narita, Modeling and characterization of the electrical conductivity of carbon nanotube-based polymer composites, Polymer. 52 (2011) 3852–3856. https://doi.org/10.1016/j.polymer.2011.06.046.
[56] J.-F. Guillet, Z. Valdez-Nava, M. Golzio, E. Flahaut, Electrical properties of double-wall carbon nanotubes nanocomposite hydrogels, Carbon. 146 (2019) 542–548. https://doi.org/10.1016/j.carbon.2019.01.090.
[57] K.J. Loh, J.P. Lynch, B.S. Shim, N.A. Kotov, Tailoring Piezoresistive Sensitivity of Multilayer Carbon Nanotube Composite Strain Sensors, Journal of Intelligent Material Systems and Structures. 19 (2008) 747–764. https://doi.org/10.1177/1045389X07079872.
[58] D.J. Yang, Q. Zhang, G. Chen, S.F. Yoon, J. Ahn, S.G. Wang, Q. Zhou, Q. Wang, J.Q. Li, Thermal conductivity of multiwalled carbon nanotubes, Phys. Rev. B. 66 (2002) 165440. https://doi.org/10.1103/PhysRevB.66.165440.
[59] J.A. Diaz, Z. Ye, X. Wu, A.L. Moore, R.J. Moon, A. Martini, D.J. Boday, J.P. Youngblood, Thermal Conductivity in Nanostructured Films: From Single Cellulose Nanocrystals to Bulk Films, Biomacromolecules. 15 (2014) 4096–4101. https://doi.org/10.1021/bm501131a.
[60] S. Frank, P. Poncharal, Z.L. Wang, W.A. de Heer, Carbon Nanotube Quantum Resistors, Science. 280 (1998) 1744–1746. https://doi.org/10.1126/science.280.5370.1744.
[61] F. Yin, D. Ye, C. Zhu, L. Qiu, Y. Huang, Stretchable, Highly Durable Ternary Nanocomposite Strain Sensor for Structural Health Monitoring of Flexible Aircraft, Sensors. 17 (2017) 2677. https://doi.org/10.3390/s17112677.
[62] L. Vertuccio, V. Vittoria, L. Guadagno, F. De Santis, Strain and damage monitoring in carbon-nanotube-based composite under cyclic strain, Composites Part A: Applied Science and Manufacturing. 71 (2015) 9–16. https://doi.org/10.1016/j.compositesa.2015.01.001.
[63] G.T. Pham, Y.-B. Park, Z. Liang, C. Zhang, B. Wang, Processing and modeling of conductive thermoplastic/carbon nanotube films for strain sensing, Composites Part B: Engineering. 39 (2008) 209–216. https://doi.org/10.1016/j.compositesb.2007.02.024.

[64] A. Santos, L. Amorim, J.P. Nunes, L.A. Rocha, A.F. Silva, J.C. Viana, Aligned carbon nanotube based sensors for strain sensing applications, Sensors and Actuators A: Physical. 289 (2019) 157–164. https://doi.org/10.1016/j.sna.2019.02.026.
[65] Y. Wang, S. Wang, M. Li, Y. Gu, Z. Zhang, Piezoresistive response of carbon nanotube composite film under laterally compressive strain, Sensors and Actuators A: Physical. 273 (2018) 140–146. https://doi.org/10.1016/j.sna.2018.02.032.
[66] A.R. Alian, S.A. Meguid, Multiscale modeling of the coupled electromechanical behavior of multifunctional nanocomposites, Composite Structures. 208 (2019) 826–835. https://doi.org/10.1016/j.compstruct.2018.10.066.
[67] W.S. Bao, S.A. Meguid, Z.H. Zhu, G.J. Weng, Tunneling resistance and its effect on the electrical conductivity of carbon nanotube nanocomposites, Journal of Applied Physics. 111 (2012) 093726. https://doi.org/10.1063/1.4716010.
[68] H.F. Castro, V. Correia, N. Pereira, P. Costab, J. Oliveiraa, S. Lanceros-Méndez, Printed Wheatstone bridge with embedded polymer based piezoresistive sensors for strain sensing applications, Additive Manufacturing. 20 (2018) 119–125. https://doi.org/10.1016/j.addma.2018.01.004.
[69] A. Ferreira, S. Lanceros-Mendez, Piezoresistive response of spray-printed carbon nanotube/poly(vinylidene fluoride) composites, Composites Part B: Engineering. 96 (2016) 242–247. https://doi.org/10.1016/j.compositesb.2016.03.098.
[70] H. Montazerian, A. Dalili, A.S. Milani, M. Hoorfar, Piezoresistive sensing in chopped carbon fiber embedded PDMS yarns, Composites Part B: Engineering. 164 (2019) 648–658. https://doi.org/10.1016/j.compositesb.2019.01.090.

Schematic 1: Preparation of CNT/CNC applied onto GFRP as paint and schematics of the testing setup.

Schematic 2: Illustration of the effective length of a CNC rod.

Figure 1: a) shear viscosity as a function of shear rate for different CNT/CNC ink compositions, b) shear viscosity as a function of total CNT and CNC concentration by fixing CNT-to-CNC ratio at 1:1 (angular frequency of 0.1 rad/s), c) storage (G′) and loss (G′′) moduli as a function of angular frequency for 0.5:0.5 and 0.8:0.8 inks, and d) comparison between shear and complex viscosities for 0.5:0.5 ink.

Figure 2: Surface morphology of developed strain sensors at different CNT/CNC compositions: a) 0.5:0.5, b) 0.8:0.4, c) 0.8:0.8, and d) 0.8:4.0. (yellow arrows show bright regions which were attributed to CNCs)

Figure 3: a) current-voltage curves for the developed sensors and b) change in sheet resistance in unloading state as a function of CNC under different temperatures.

Figure 4: a) stress-strain graph, and experimental and theoretical tensile piezoresistive behavior of b) CNT/CNC@0.5:0.5, c) CNT/CNC@0.8:0.4, d) CNT/CNC@0.8:0.8, and e) CNT/CNC@0.8:4.0.

Figure 5: a) change in tunneling distance and b) tunneling distance as a function of strains at various CNC compositions.

Figure 6: Effect of CNCs, at low and high loads, on the type of conductive CNT conductive paths.

Figure 7: Piezoresistive behavior as a function of time for a total of 250 cycles for CNT/CNC@0.8:0.8 at a strain of 0.60%. Inset figure shows enlarged portion of change in resistance at time interval between 3500 and 4120 second.

Table 1: Sample identification for developed CNT/CNC inks and abbreviations.

Table 2: Constants and parameters used in this study for modeling.

Table 3: Rheological properties of CNT/CNC inks at varying weight ratios.

Table 4: Properties and characteristics of the CNT/CNC strain sensors.